Journal Name

ARTICLE

Robust electrografted interfaces on metal oxides for electrocatalysis - an *in situ* spectroelectrochemical study

Received 00th January 20xx,
Accepted 00th January 20xx

DOI: 10.1039/x0xx00000x

www.rsc.org/

Tomos G.A.A Harris[1,2], Robert Götz[1,3], Pierre Wrozlek[4], Victoria Davis[2], Caroline E. Knapp[5], Khoa Ly[6], Peter Hildebrandt[1], Matthias Schwalbe[4], Inez Weidinger[3], Ingo Zebger[1], Anna Fischer[2]

Diazonium salts were electrografted onto transparent conductive oxides as stable alternatives to conventional anchoring groups for the surface immobilisation of molecular species, such as molecular electrocatalysts and / or photosensitisers. Surface sensitive *in situ* ATR-IR spectroscopy, in combination with spectroelectrochemistry, was used as tool to provide unprecedented information on the interface formation, structure and stability, which is not possible using conventional approaches. Electrografted interfaces deposited on model oxides were thereby shown to be stable in an extraordinarily wide pH range (2.5 – 12) and electrochemical potential window (-0.73 to 2.23 V vs RHE in aqueous media, and -1.3 V to 1.6 V vs Fc/Fc^+ in organic media). As a model electrocatalyst, an Fe porphyrin active for the oxygen reduction reaction (ORR) was immobilised on both mesoporous antimony doped tin oxide (me-ATO) and planar tin doped indium oxide (pl-ITO) using this electrografting approach. Surface coverages comparable to those previously reported using phosphonate anchoring groups were achieved. In addition, fast electron transfer rates were demonstrated, while *in situ* resonance Raman spectroelectrochemistry proved the co-ordination of the immobilised species and demonstrated its excellent electrochemical accessibility.

Introduction

The storage of (renewable) energy in the form of chemical bonds in electrofuels and chemical feedstocks will play a crucial role in the decarbonisation of the economy.[1] To achieve this, efficient catalysts that promote the interconversion between electrical and chemical energy in an economic manner must be developed. Homogenous molecular electrocatalysts only require a few metal atoms to catalyse a reaction, while also offering the possibility of facile chemical 'fine tuning' of the first and second coordination sphere that can help circumvent energy scaling relations found in heterogeneous catalysts.[2,3] Structure-reactivity relationships can thus be more easily investigated, especially in combination with in-depth analysis of reaction mechanisms using spectroscopic techniques, which facilitates rational catalyst design.[4]

In the context of electrocatalysis, the immobilisation, or grafting, of molecular catalysts on electrode surfaces is imperative, thereby increasing the number of addressable active sites, promoting electron transfer to and from the electrode, facilitating the use of aqueous solvents, and preventing crossover of diffusing catalysts between the cathode and anode.[5] Immobilisation can be carried out on semiconducting metal oxides, taking advantage of their low cost and allowing the combination of catalytic properties with certain electrode properties e.g. stability under highly anodic potentials (i.e. for water oxidation), high surface areas due to nanostructuration, and transparency in the case of transparent conductive oxides (TCOs); the latter facilitating light-induced processes and spectroscopic investigations. Besides TCOs, dye sensitised or narrow band gap semiconductors can be used for solar energy conversion purposes.[6]

For surface immobilisation of molecular electrocatalysts or photosensitisers on oxides, hitherto used anchoring groups include phosphonates, carboxylates, silanes and their derivatives (e.g. silatranes), amongst others.[7–15] While each has its own merits in terms of stability and charge transfer properties, one usually comes at the expense of the other.[16–18] For example, phosphonate and carboxylate anchoring groups readily desorb in the alkaline pH's favoured for the oxygen evolution reaction (OER) and oxygen reduction reaction (ORR) when catalysed by non-precious metal compounds. Furthermore, the electrochemical stability of such non-covalent binding motifs is poor. As such, new immobilisation approaches must be developed that, in practical terms, are (1) robust enough to withstand a range of chemical and electrochemical

[1] *Technische Universität Berlin, Institut für Chemie, PC 14, Str. des 17. Juni 135, 10623 Berlin, Germany*
[2] *Albert-Ludwigs-Universität Freiburg, Institut für Anorganische und Analytische Chemie, Albertstr. 21, 79104 Freiburg, Germany*
[3] *Technische Universität Dresden, Fachrichtung Chemie und Lebensmittelchemie, Helmholtzstr. 10, 01069 Dresden, Germany*
[4] *Humboldt Universität zu Berlin, Institut für Chemie, Brook-Taylor-Strasse 2, 12489 Berlin, Germany*
[5] *Department of Chemistry, University College London, 20 Gordon Street, London, WC1H 0AJ, United Kingdom*
[6] *Department of Chemistry, University of Cambridge, Lensfield Road, CB2 1EW, Cambridge, United Kingdom*
† Footnotes relating to the title and/or authors should appear here.
Electronic Supplementary Information (ESI) available: Experimental details and synthetic procedures. Fig S1-S22, and Tables S1-S3. See DOI: 10.1039/x0xx00000x

Please do not adjust margins

conditions, (2) facilitate efficient and fast charge transfer and (3) are synthetically straightforward to realise.

Aryl diazonium salts have been widely used to functionalise a range of electrode materials *via* chemical or electrochemical grafting (electrografting), including carbon materials[19–24], metals[25], and semiconductors like silicon[26]. Electrografting is a particularly powerful and versatile technique, often resulting in very strong covalent bonds between the electrode substrate and the modifier.[27] More recently, the electrografting of diazonium salts has been demonstrated on metal oxides, and it has been proposed that phenyl radical species (which are formed during the electrografting reaction) form covalent M-O-C bonds at the interface of the oxide.[28,29] Despite this, few examples exist where metal oxide materials have been functionalised in this way, including TiO_2,[29–31] indium tin oxide (ITO),[24,31–34] and fluorine-doped tin oxide (FTO).[35] Moreover, the stability of diazonium-derived interfaces on metal oxides has not been addressed so far; an aspect which is crucial for robust interface development.

In the present work, we explored the applicability of diazonium electrografting for the stable and covalent immobilisation of molecular species on TCOs, using mesoporous antimony-doped tin oxide (me-ATO) and planar ITO (pl-ITO) as model oxide platforms. We recently developed a spectroelectrochemical approach for determining the electrochemical stability window of electrografted diazonium interfaces on Au electrodes using *in situ* surface enhanced infrared absorption spectroscopy in attenuated total reflection (ATR) mode, with plasmonic enhancement of the signal due to the nanostructuration of the Au.[36] Extending our approach to TCOs with high surface areas like me-ATO (and thereby increasing surface sensitivity in the absence of plasmonic enhancement) provides unprecedented information on interface formation, structure and stability, thus allowing both the hydrolytic and electrochemical stability window of these interfaces (and other anchoring groups) to be determined. Previous attempts to probe the stability of anchoring groups on oxides have relied on UV-Vis spectroscopic or solely electrochemical techniques.[12,14,18,37,38] *In situ* IR spectroscopy on the other hand allows the intrinsic stability of an anchoring group to be determined without relying on chromophoric or electroactive components (which may themselves be unstable). As a model electrocatalyst, an Fe 'hangman' porphyrin active for the ORR was immobilised. In addition to electrochemical methods, *in situ* resonance Raman (rR) spectroelectrochemistry was used to characterise the immobilised species and determine their electrochemical accessibility.

Results and discussion

Interface formation and characterisation

me-ATO (8% Sb-doping) thin films were deposited on ITO glass slides by evaporation induced self-assembly of preformed ATO nanoparticles (approx. 4 nm in diameter, see Fig. S1) in the presence of the block co-polymer F127, as previously described by our group.[39] ATO is highly conductive, transparent, resistant to corrosion, and has been used for many purposes including as conductive supports for electrocatalysis.[39–44] As evidenced by SEM (Scheme 1, for further magnifications see Fig. S2), the resulting crack-free me-ATO films are around 160 nm thick with an open, mesoporous structure throughout (pore size ~ 8 nm, as determined previously[39]). Many examples exist in literature where electrode films were prepared from dispersions of commercial ITO or ATO powders (crystallite size ~ 50 nm)[45,46], resulting in very thick (up to several µm) albeit turbid films. On the contrary, the thin films synthesised in this study exhibit excellent transparency as a result of their small crystallite and pore size that reduces scattering, thus making them especially suitable for *in situ* spectroscopic studies.

Successful electrografting of the me-ATO surface is indicated by comparative CV measurements in the presence of the ferrocene/ferrocenium (Fc/Fc^+) redox probe of me-ATO electrodes before and after electrografting (Fig. S3): in addition to a slight increase in peak separation between the anodic and cathodic wave (ΔE_P), a significant decrease of 52% in the ferrocene oxidation current is observed. Successful interface formation can further be observed in XPS measurements conducted on me-ATO before and after electrografting, as shown in Fig. 1. For details on the fitting procedure, as well as the C 1s and Sn 3d spectra, and the tabulated binding energies (BE) of the deconvoluted components of the N 1s and O 1s spectra, see the Fig. S4 and Table S1. The N 1s spectra of me-ATO after electrografting show peaks at 399.2 and 401.1 eV that are assigned to the amine and imine nitrogen environments of the deposited interface. The peak at 402.1 eV is assigned to the iminium environment that results from protonation of imine

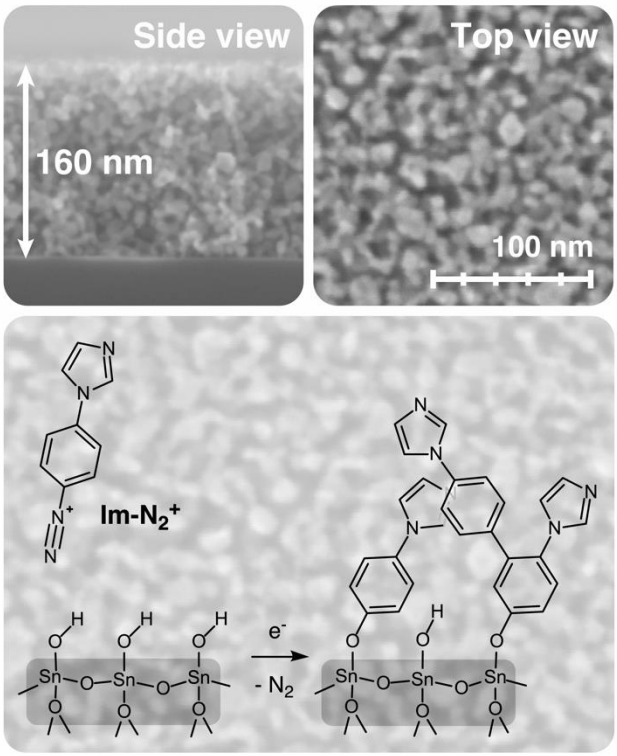

Scheme 1 Top view and cross-sectional SEM images of me-ATO thin films showing both the mesostructure and the film thickness. Below: Schematic representation of the electrografting of the diazonium salt Im-N_2^+ onto the surface of the ATO (Sb-doped SnO_2 - Sb atoms omitted for clarity).

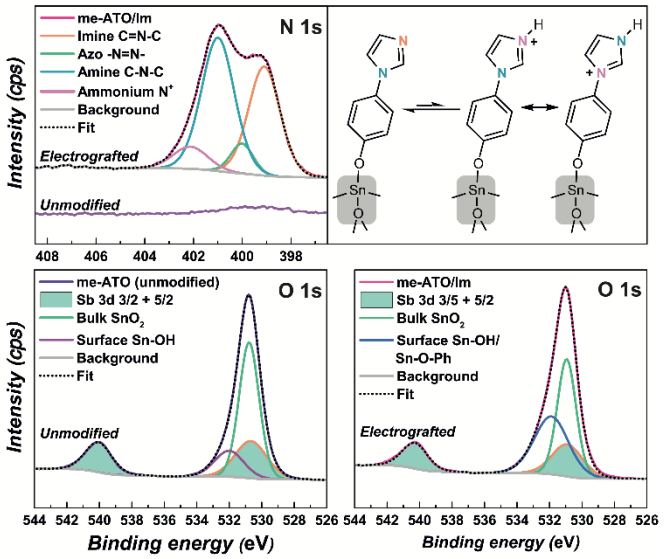

Figure 1 Deconvoluted N 1s and O 1s XPS spectra of the me-ATO before and after electrografting with Im-N_2^+. The colour coordinated scheme (top right) indicates the different nitrogen envrionments present.

nitrogen, representing a shift in BE of 2.8 eV. Summing together the atomic percentages of imine and iminium nitrogen results in an almost 1:1 ratio with the amine nitrogen, as expected for imidazole, and suggests that around 14% of the interface is protonated. A small peak at 400.1 eV is assigned to azo-bridges that may form as a result of the limited addition of non-reduced diazonium ions to already-grafted species.[47] In the O 1s spectra, the ratio between the peak at 530.8 eV, attributed to the bulk lattice oxygen component, and the peak at 532 eV, attributed to surface Sn–OH, decreases after electrografting; however, it was not possible to discriminate the presence of any Sn–O–C bonds due to their similar BE, reported to be 532.2 eV.[48]

The high surface area of the me-ATO results in high IR absorption intensities for adsorbed species in ATR mode that can provide unprecedented information on interface formation and structure. For that, a silicon-prism was coated with a me-ATO thin film *via* spin-coating (for details see SI) and *in situ* IR spectroelectrochemical measurements were performed in acetonitrile (0.1 M $TBAPF_6$ or $TBAClO_4$) using a Kretschmann ATR configuration. Upon addition of 1 mM Im-N_2^+ to the spectroelectrochemical cell, a band at 2253 cm^{-1} appears in the IR adsorption spectrum (Fig. 2), corresponding to the diazonium N≡N stretching vibration ν(N≡N), in addition to bands corresponding to vibrations of the phenyl-imidazole moiety, thus indicating the adsorption of Im-N_2^+ species onto the ATO surface. The ν(N≡N) band is partially obscured by two negative δ(CCN) and ν(C≡N) bands resulting from the displacement of acetonitrile molecules from the surface (asterisked). Meanwhile, a further negative $\nu_{sym}(CH_3)$ band for acetonitrile is observed at 1375 cm^{-1} (for an ATR-IR spectrum of me-ATO in acetonitrile see Fig. S6). After this initial rapid adsorption, further growth in band intensity due to the spontaneous heterolytic decomposition of diazonium species is small in comparison. Upon electrochemical reduction, the ν(N≡N) band disappears, and bands such as the ones at 1608 cm^{-1} corresponding to the aromatic $\nu(C=C)_{ph}$ mode of the phenyl ring, and 1515 cm^{-1} corresponding predominantly to the coupled δ(C-H), $\nu(C=C)_{ph}$ and ν(C-N) modes of the deprotonated imidazole ring, increase significantly in intensity. These phenyl-imidazole-specific absorption intensities are resistant to repeated rinsing in multiple solvents, strongly indicating that the interface is covalently attached to the ATO surface.

As previously mentioned, it is anticipated that electrografting of diazonium salts will result in the formation of M-O-C bonds (in this case Sn-O-C) at the interface. In order to model such surface-bound species, an IR spectrum of **1**, a phenyl-imidazole species bound *via* a Sn-O-C bond to a $Sn(OH)_3$ cluster, was calculated using DFT. There is a good agreement between the experimental spectrum and the spectrum calculated using this monoatomic tin model, which is smaller

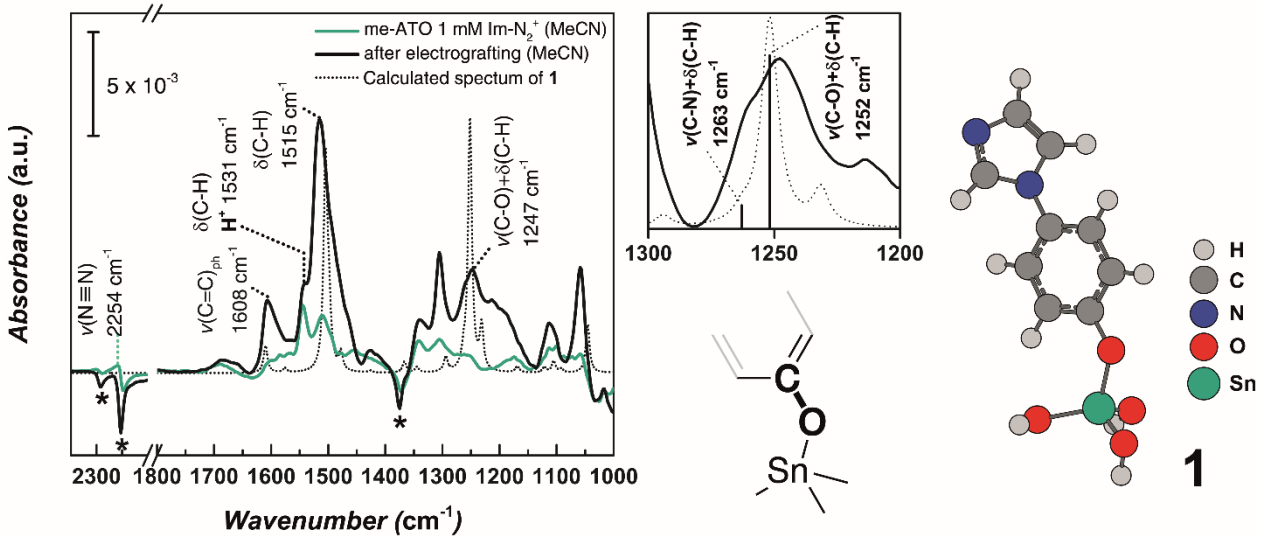

Figure 2 *In situ* IR spectrum recorded in ATR mode of me-ATO in a 1 mM solution of Im-N_2^+ in acetonitrile (0.1 M $TBAPF_6$) before electrografting is shown in dark green. The corresponding spectrum in fresh acetonitrile (without Im-N_2^+) after electrografting is shown in black. On the right is the optimised structure of Im-$Sn(OH)_4$ (**1**), atom labels: carbon (dark grey), hydrogen (light grey), nitrogen (blue), oxygen (red), tin (green). The corresponding IR spectrum of **1** calculated using DFT is shown in black (dotted line). The inset displays the overlapping bands at 1247 cm^{-1} (× 4), overlaid with calculated contributions from ν(C-N)+δ(C-H) and ν(C-O)+δ(C-H) modes. Negative bands resulting from the displacement of acetonitrile molecules from the surface after addition of Im-N_2^+ and subsequent electrografting are asterisked.

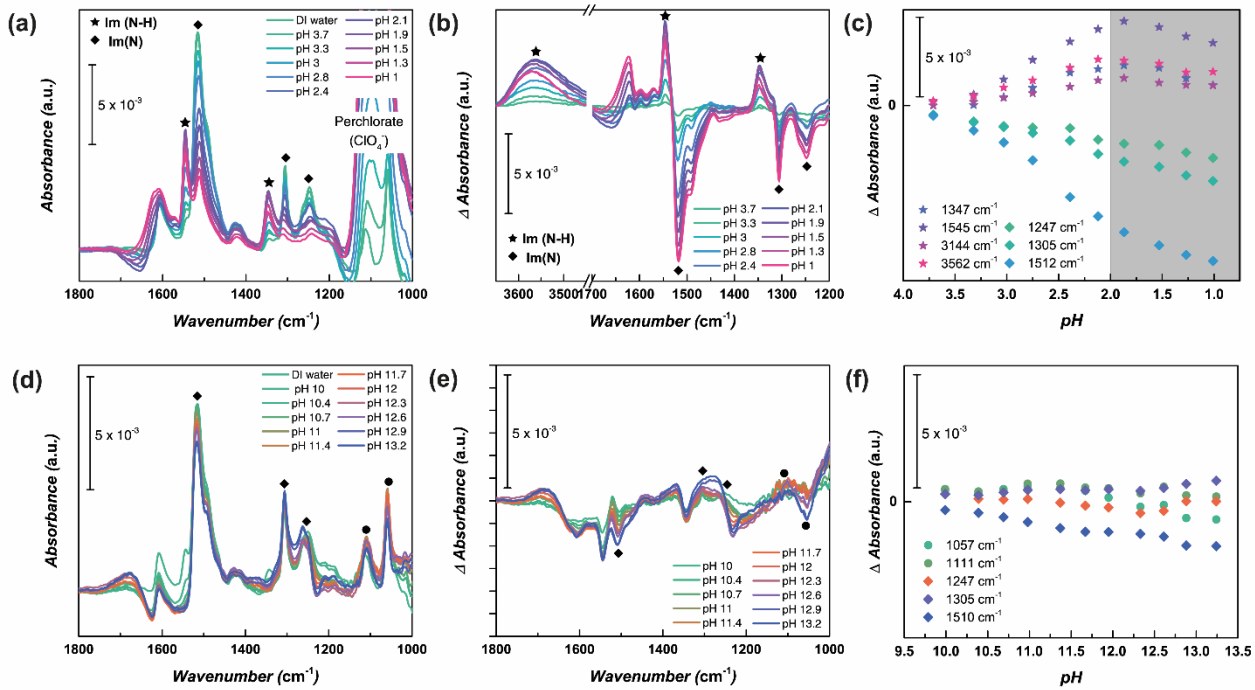

Figure 3 (a) *In situ* IR spectra recorded in ATR mode of the electrografted diazonium interface on me-ATO in increasingly acidic $HClO_4$ solutions, and (b) difference spectra showing the change in absorbance ΔA at each pH with respect to the initial spectrum of the interface in deionised (DI) water. (c) Plot of ΔA as a function of pH with bands marked with stars or diamonds corresponding to vibrational modes of the protonated **Im(N-H)** or de-protonated **Im(N)** species, respectively. (d), (e) and (f) show the corresponding absorbance and difference spectra, as well as a plot of ΔA as a function of pH, for the electrografted interface in increasingly basic KOH solutions. The bands marked with circles correspond to vibrational modes common to both Im(N-H) and Im(N) species.

than the larger 9 Ti atom model recently employed by Brudvig and co-workers to model molecular species bound to TiO_2.[11] The inset in Fig. 3 shows the two overlapping bands at 1247 cm^{-1} that correspond to the ν(C-N)+δ(C-H) and ν(C-O)+δ(C-H) modes calculated for **1**. This supports the assumption that the phenyl radicals bind to surface hydroxyl groups forming covalent interfacial Sn-O-C bonds.

Interface stability

pH dependent spectroscopic stability measurements were conducted in basic and acidic solutions of KOH and $HClO_4$ to determine the hydrolytic stability window of the electrografted interfaces, which is of paramount importance in catalytic applications (Fig. 3). In both cases, difference spectra at each pH were calculated with respect to the initial spectra recorded for the interfaces in deionised water (pH ~ 6), therefore indicating the overall change in absorbance ΔA at each pH.

Upon decreasing the pH of the solution, there is a substantial change in the IR absorbance spectrum of the electrografted species. With the help of DFT calculations, these changes were assigned to the protonation of the terminal imine nitrogen of the imidazole ring (see Fig. S7). In particular, a prominent and broad band appears at 3562 cm^{-1} corresponding to N-H stretching mode ν(N-H) of the protonated species. Due to the dynamic changes taking place upon decreasing the pH, ΔA was plotted as a function of decreasing pH (Fig. 3c), allowing any desorption of linker molecules to be measured. Initially, there is an increase in ΔA for the protonated Im species (marked by stars), accompanied by a concomitant decrease for the de-protonated species (marked by diamonds). An inflection point is reached at around pH 2, beyond which there is an overall decrease in ΔA for all species, indicating that the desorption of electrografted species from the ATO surface is taking place. On closer inspection, the plots exhibit a sigmoidal shape

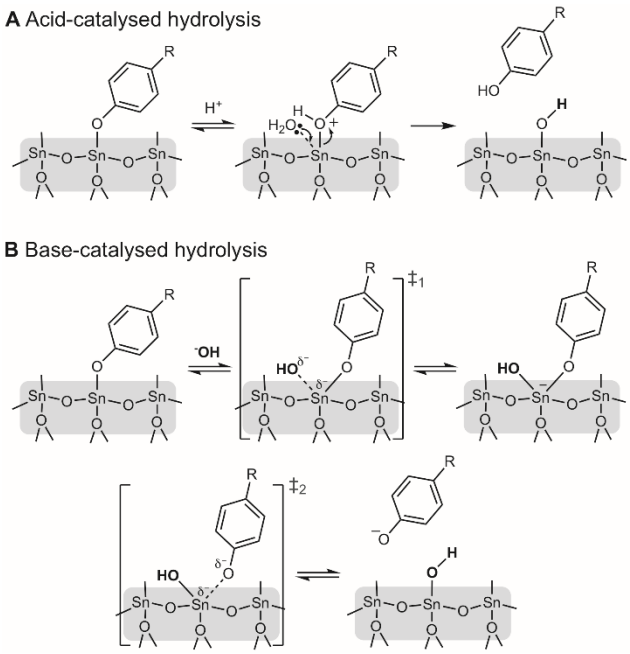

Scheme 2 Schematic representation of possible mechanisms for (**A**) acid-catalysed and (**B**) base-catalysed hydrolysis of electrografted diazonium interfaces on oxide materials, such as ATO.

characteristic of a pH titration, which is disrupted at lower pH's due to desorption (see Fig. S8).

Upon increasing the pH of the solution, a small overall decrease in the band intensities corresponding to both the protonated and de-protonated imidazole species can be observed. The spectra stabilise before slow desorption takes place at very high pH's (> pH 12). Note: shifts in the baseline take also place as the pH changes.

Spectroelectrochemical titrations were carried out in a similar fashion to determine the electrochemical stability window of the electrografted interface in a pH 7 0.1 M phosphate buffer (PB). Spectra were recorded under a potential of 0.79 V (vs RHE) after application of increasingly positive or negative potential steps (Fig. 4a and b). The absorption intensity of two bands at 1247 and 1306 cm^{-1} are plotted as a function of potential (insets Fig. 6) and a minimal decrease in intensity over

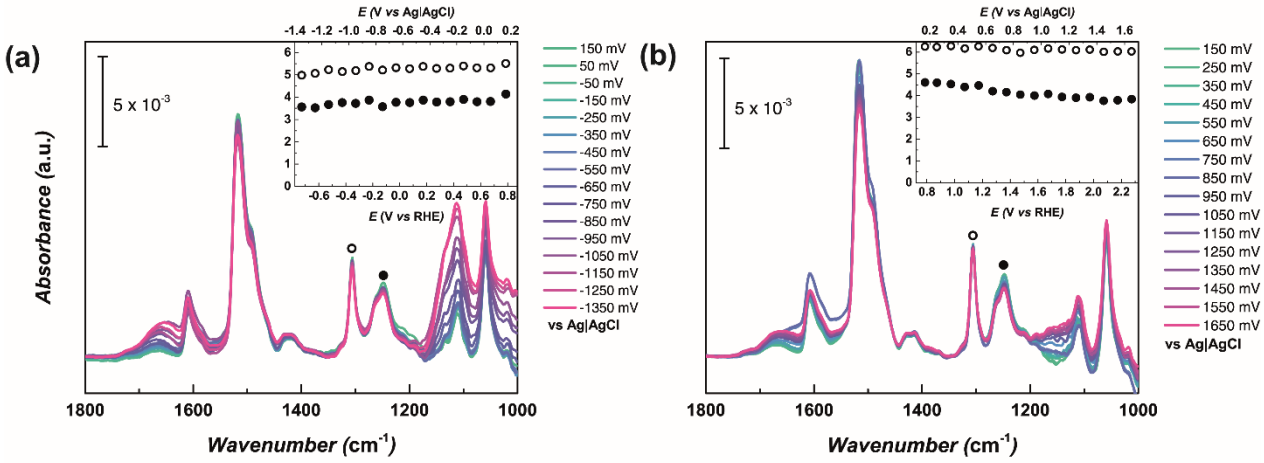

Figure 4 *In situ* IR spectra recorded in ATR mode in pH 7 (0.1 M PB) at 163 mV (vs Ag/AgCl 3M) of the electrografted interfaces on me-ATO after 2-minute-long applications of increasingly (a) cathodic or (b) anodic potential steps. Inset: plots of the indicated band intensities at 1247 and 1306 cm^{-1} as a function of applied potential.

To gain further insight into the underlying hydrolytic processes taking place under highly acidic and basic conditions, IR absorption spectra of electrografted interfaces were recorded in 0.1 M $HClO_4$ (pH 1) and 0.1 M KOH (pH 12.8). In each case, the decrease in absorbance was plotted as a function of time (Fig. S9), where absorbance is proportional to the concentration of molecules grafted at the interface. Hydrolysis in 0.1 M KOH appears to exhibit (pseudo-) first-order kinetics with an apparent hydrolysis rate $k_{hyd} = 3.77 \times 10^{-5} \pm 0.34\ s^{-1}$, which corresponds to a half-life of 5.5 hours. In 0.1 M $HClO_4$, a higher-order reaction takes place. Assuming hydrolysis of interfacial Sn-O-C bonds, a classical S_N2-type hydrolysis is not expected to take place in either case due to the impossibility of symmetry inversion at the interface. A more plausible mechanism for acid-catalysed hydrolysis involves flank-side attack of the Sn atom by a water molecule *without* inversion of symmetry, in which the oxygen atom is first protonated in a rate determining step, as illustrated by mechanism A in Scheme 2. A possible mechanism for base-catalysed hydrolysis may involve an attack of the Sn atom by a hydroxide anion, resulting in the formation of a 5-coordinate intermediate and the subsequent displacement and removal of the phenoxide anion (mechanism B in Scheme 2). Similar mechanisms have been proposed for the hydrolysis of silicates[49], where Si has a similar Lewis acidity as Sn. It is anticipated that hydrolysis rates will differ depending on the nature of the metal atom (e.g. Sn/Sb/In/Ti etc.), the crystallographic facet to which the phenyl species is bound to, as well as the diazonium salt used, i.e. due to inductive effects depending on the phenyl-substituents (in this case imidazole-1-yl).

the measured potential ranges is observed, which is attributed to the previously reported loss of physisorbed species deposited during electrografting[50], as well as shifts in the baseline (these are more pronounced at low wavenumbers). In contrast to electrografted interfaces on Au, where we observed the electrochemical cleavage of the Au–C interfacial bond as a rapid decrease in IR absorption intensity[36], the electrografted interfaces on ATO are stable in a broad potential window (at least -0.73 to 2.23 V vs RHE) that encompasses the intrinsic electrochemical stability windows of ATO at pH 7 (-0.77 to 1.83 V vs RHE, for measurement see Fig. S10) as well as FTO and ITO in neutral electrolyte (-0.62 to 1.96 V vs RHE and -0.51 to 1.73 V vs RHE, respectively[51]). Measurements in organic media (acetonitrile, 0.1 M $TBAClO_4$, see Fig. S11) indicate a similarly broad stability window (-1.3 to 1.6 V vs Fc/Fc^+) with desorption observed at potentials more cathodic than -1.3 V.

Immobilisation of a model catalyst and redox behaviour

As the name suggests, hangman porphyrins (depicted in scheme 3) contain a 'hanging' group positioned at a fixed distance from the metal centre (i.e. in the second coordination sphere of the complex), which may introduce certain non-covalent interactions, such as proton coupled electron transfer, and can alter the catalytic activity of a complex.[52,53] Carboxylic acid hanging groups on molecular complexes have been shown to enhance the catalytic activity of reactions including the ORR, H_2O_2 reduction and the OER.[53–57] The porphyrin containing the methyl ester hanging group (FePOMe) was used in this study to rule out the influence of pH on the ORR onset potential[56], as

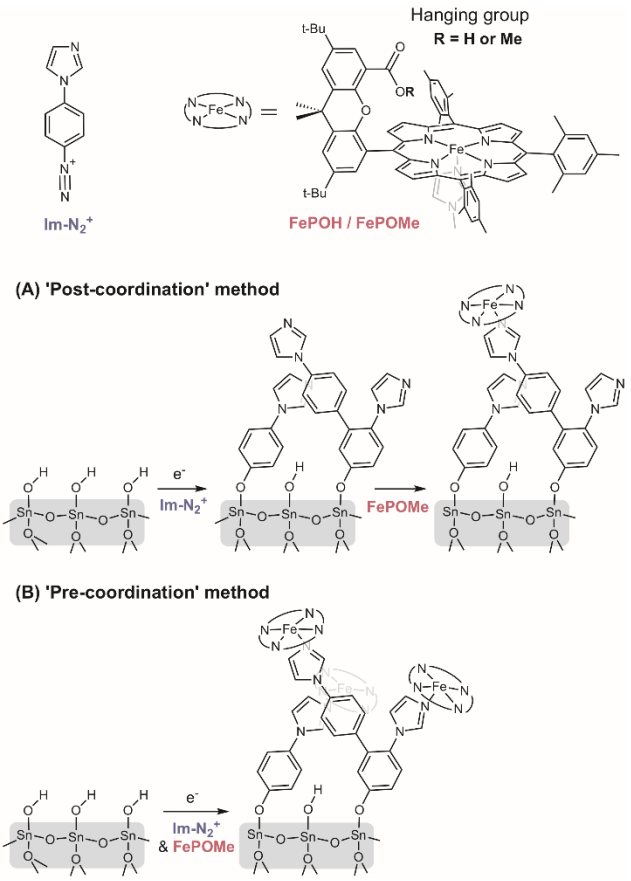

Scheme 3 Top: structure of the iron hangman porphyrin. Bottom: schematic overview of the two methods used to immobilise FePOMe on the surface of the ATO: (A) *via* the two-step 'post-coordination' process, or (B) *via* the one-step 'pre-coordination' process.

well as to exclude the possibility of the porphyrin binding to the oxide *via* the carboxylic acid hanging group.

Two distinct immobilisation methods were employed: (A) a two-step 'post-coordination' process whereby the me-ATO already electrografted with Im–N_2^+ was incubated with FePOMe, and (B) a one-step 'pre-coordination' process whereby me-ATO was electrografted with a mixture of Im–N_2^+ and FePOMe together in acetonitrile, after a mixing time of 5 min to allow pre-coordination of the Im–N_2^+ to the Fe centre. In both cases a potential of -0.42 V (vs Fc/Fc^+) corresponding to the reduction potential of Im–N_2^+ (see CV Fig. S12) was applied for 120 s. Both processes result in a dark brown colouration of the electrode that is resistant to repeated rinsing and soaking in acetonitrile and dichloromethane (see photograph Fig. S13). Surface coverages of FePOMe Γ_{UV} of 1.5 and 3.9 × 10^{-9} molcm^{-2} were determined by UV-vis spectroscopy for the 'post-coordination' and 'pre-coordination' methods, respectively.

CVs in acetonitrile (0.1 M $TBAClO_4$) of the modified electrodes stabilise over several cycles and show a reversible redox peak close to -0.56 V (vs. Fc/Fc^+) assigned to the Fe^{2+}/Fe^{3+} redox couple of the immobilised FePOMe (Fig. 5). Peak currents (I_P) increase linearly with applied scan rate, as expected for a surface-bound redox species (see Fig. S14 and S15). Surface coverages of electroactive FePOMe Γ_{CV} of 1.5 and 3.0 × 10^{-9}

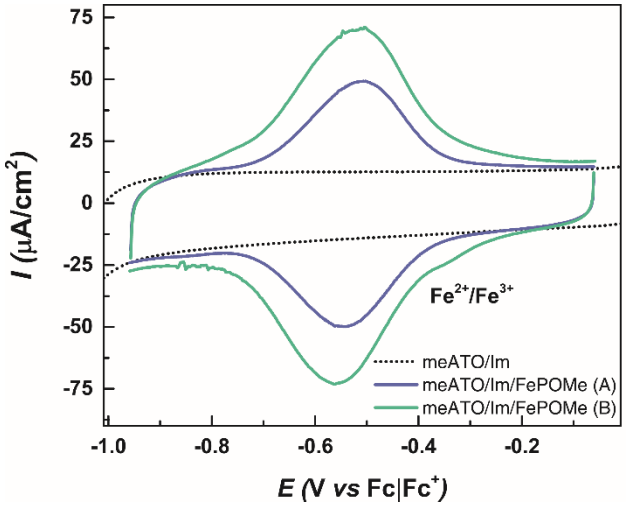

Figure 5 CVs in acetonitrile (0.1 M $TBAClO_4$) of FePOMe immobilised on me-ATO using the 'post-coordination' method (labelled A, blue trace) and 'pre-coordination' method (labelled B, green trace). Scan rate = 50 mVs^{-1}.

molcm^{-2} were calculated from background subtracted CVs for the 'post-coordination' and 'pre-coordination' methods, respectively. The ratio between Γ_{CV} and Γ_{UV} suggest that all of the species immobilised using the 'post-coordination' method are electroactive, while around 75% of the species immobilised using the 'pre-coordination' method are electroactive. The coverages obtained are in line with those reported in literature for molecular catalysts immobilised on other porous oxide electrodes using phosphonate or silane anchoring groups when taking into account differences in thicknesses (as loading increases linearly with film thickness). These comparisons are summarised in Table S2.

Full-widths at half maximum (FWHMs) E_{FWHM} of the oxidation and reduction waves, accounting for 199 and 197 mV for 'post-coordination', and 210 and 211 mV for 'pre-coordination', respectively, are found to be greater than the theoretical 90.6 mV[58] expected for a 1-electron transfer process. This broadening results from electrostatic intermolecular interactions between immobilised species,[59,60] with a higher loading of FePOMe leading to a broader FWHM, as previously observed for porphyrins immobilised on Si.[61] In addition, broadening of the FWHM may reflect a certain heterogeneity in the immobilised species. These results that suggest the 'pre-coordination' method results in more crowded, or multi-layer configurations of FePOMe attached to the ATO surface.

Fe^{2+}/Fe^{3+} peak separations ΔE_P at 10 mVs^{-1} for me-ATO electrodes modified using the 'post-coordination' and 'pre-coordination' methods are small (26 mV and 32 mV, respectively), while at higher scan rates they deviate from a linear relationship, indicating a kinetic limitation (Fig. S16). The apparent electron transfer (ET) rate constants k_c and k_a, as well as the ET coefficients α_c and α_a, were calculated for the cathodic and anodic peaks using mathematical treatments derived by Laviron.[62] 'Post-coordination' resulted in k_c = 4.4 ± 0.7 s^{-1}, α_c = 0.62, k_a = 2.9 ± 0.1 s^{-1} and α_a = 0.28, while 'pre-coordination' gave k_c = 4.9 ± 0.1 s^{-1}, α_c = 0.81, k_a = 2.8 ± 0.1 s^{-1} and α_a = 0.14.

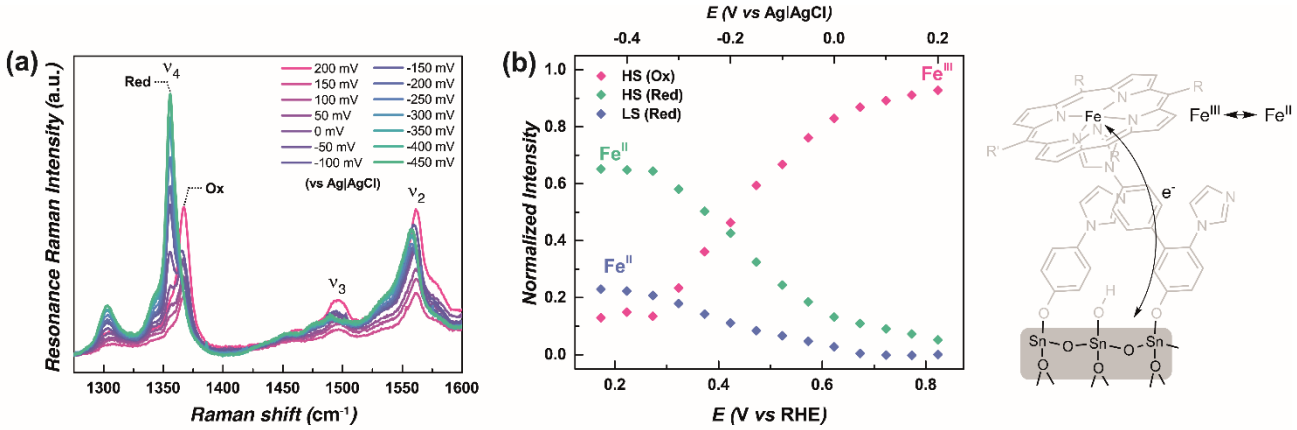

Figure 6 (a) *In situ* potential-dependent resonance Raman (rR) spectra recorded in pH 7 (0.1 M PB) of FePOMe immobilised on me-ATO and (b) the relative contributions from the different FePOMe spectra components at different potentials.

The unsymmetrical energetic barrier for ET, as indicated by α, can be explained by crowding of the immobilised species or structural changes upon changes in oxidation state. The ET rates calculated here are in line with those obtained for other redox systems immobilised on nanostructured metal oxides. Further comparisons to literature are given in Table S3. It is highly likely that ET rates for redox species immobilised in such porous electrode films are restricted due to lower charge carrier mobility/resistivity in the narrow pore walls, or increased reorganisation energies e.g. due to the limited diffusion of counterions into the Helmholtz layer of the high surface area electrode. In fact, a two-order magnitude decrease in ET rate has been observed for Hemin immobilised on multiwalled carbon nanotubes (MWCNTs) compared to planar glassy carbon.[63,64]

The high loadings of FePOMe on me-ATO results in very high resonance Raman (rR) scattering intensities, allowing the co-ordination, redox and spin states of the porphyrin to be easily ascertained. *In situ* rR spectroelectrochemical measurements of FePOMe immobilised using the 'post-coordination' method were performed in pH 7 (0.1 M PB) under different potential steps (Fig. 6a) and component fit analysis was carried out to decompose each potential-dependent spectrum into the different contributing redox and conformational components (Fig. 6b), as described elsewhere in detail for Hangman species immobilized on SAM-coated silver electrodes by Ly et al.[56] At OCP (135 mV vs Ag/AgCl 3M KCl), intense marker bands appear around 1367 cm^{-1} (ν_4) and 1561 cm^{-1} (ν_2) with a lower intensity band at around 1495 cm^{-1} (ν_3). The main spectral contribution arises from the Fe^{3+} 5-coordinated high-spin (HS) state of the FePOMe, with a small contribution from the 6-coordinated low-spin (LS) state, as evidenced by a high-frequency shoulder in the ν_3 band at 1502 cm^{-1}. This indicates that most of the immobilised hangman species are axially coordinated to the surface *via* the imidazole linker with a 6th coordination site free for oxygen binding. 6-coordinated species were also observed by Ly et al. and their molecular origin is at present unknown. Plotting the different contributions as a function of applied potential allows the reduction of the immobilised Fe^{3+} species to be spectroscopically followed, and hence their electrochemical accessibility to be evaluated. There is an almost complete reduction in intensity of the Fe^{3+} state, proving that almost all of the immobilised species are indeed electroactive (i.e. electrocontacted), despite passivation of the me-ATO during electrografting.

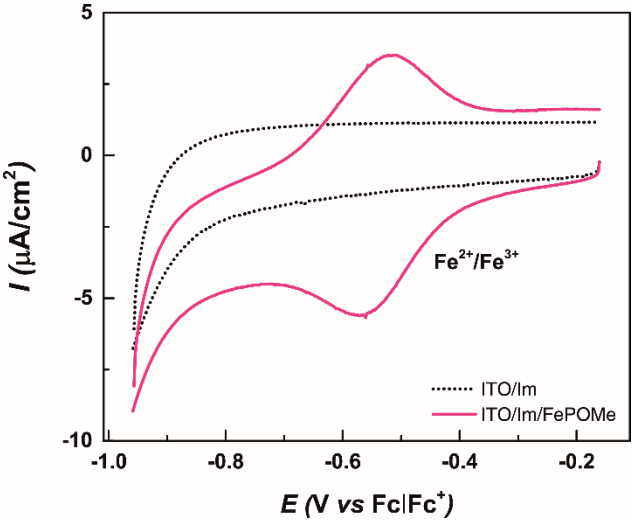

Figure 7 CVs in acetonitrile (0.1 M $TBAClO_4$) of FePOMe immobilised on pl-ITO using the 'post-coordination' method. Scan rate = 50 mVs^{-1}.

When electrografting was performed on a planar surface, namely planar ITO (pl-ITO), an FePOMe coverage Γ_{CV} of 1.2×10^{-10} mol cm^{-2} was obtained using the 'post-coordination' method (Fig. 7). This coverage is equivalent to 29% of a perfectly packed monolayer of FePOMe (4.2×10^{-10} $molcm^{-2}$ – as calculated from the porphyrin dimensions[52]), and is in line with coverages obtained in literature for molecular catalysts immobilised on planar ITO and FTO using phosphonate anchoring groups, whose deposition is self-limiting.[40,65,66] Analogous to me-ATO, I_P for the immobilised FePOMe Fe^{2+}/Fe^{3+} couple increases linearly with the scan rate (Fig. S17). Interestingly, ΔE_P remains constant at approximately 45 mV from a scan rate of 10 mV/s up to 500 mV/s (Fig. S18). Faster measurements could not be carried out, meaning a kinetically limited k_{ET} could not be calculated; however, it is clear that ET is very fast using these covalently grafted interfaces. Comparative measurements of a carboxylic acid anchoring group on pl-ITO and me-ATO using 4-(1H-

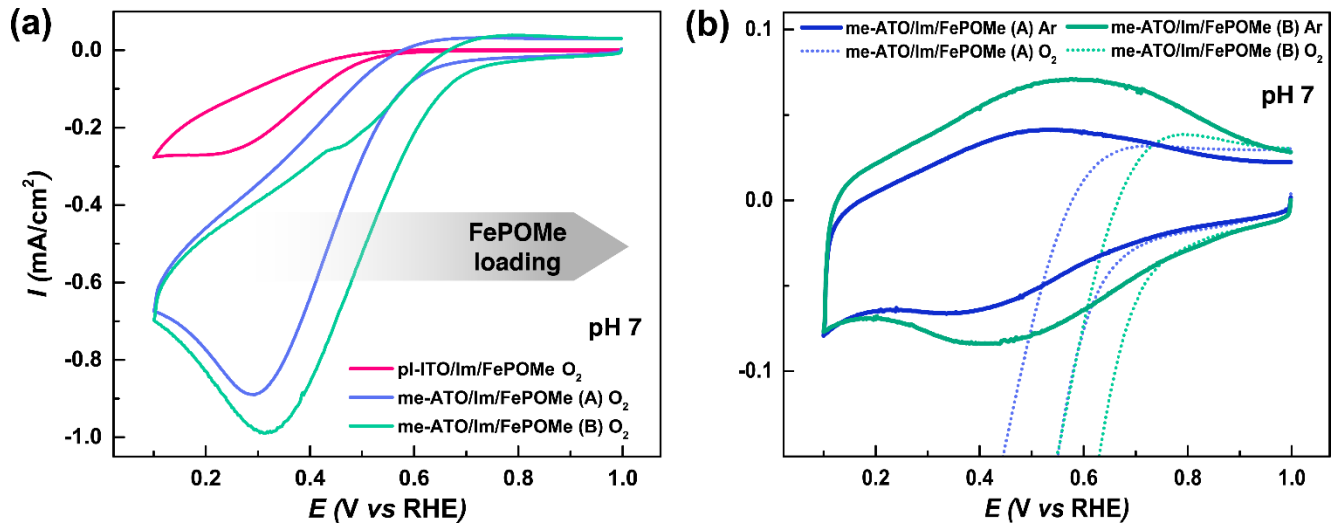

Figure 8 (a) CVs of pI-ITO and me-ATO electrodes in pH 7 (0.1 M PB) under O_2 bubbling with increasing loadings of immobilised FePOMe, and (b) CVs of the same FePOMe species immobilised on me-ATO under Ar bubbling showing the Fe^{2+}/Fe^{3+} redox couple overlaid with CVs under O_2.

Imidazol-1-yl)benzoic acid failed, presumably due to the instability of the anchoring group.

Electrocatalysis and the influence of catalyst loading

To evaluate the electrochemical performance of the FePOMe modified electrodes under ORR conditions, CV's were recorded at pH 7 (0.1 M PB) as shown in Fig. 8a. A comparison of CVs of unmodified and modified me-ATO under O_2 are shown in Fig. S19, indicating that the immobilised FePOMe is catalytically active. The FePOMe modified electrodes showed improved onset potentials for the ORR with increasing coverages of electroactive FePOMe (i.e. catalyst loading) in the order me-ATO 'pre-coordination' > me-ATO 'post-coordination' > pI-ITO 'post-coordination', with onset potentials of around 645 mV, 570 mV and 500 mV (vs RHE), respectively. Maximum diffusion limited currents of 0.9 and 1 mA/cm^2 were obtained for the 'post-coordination' and 'pre-coordination' methods, respectively.

Overpotentials for ORR have previously been shown to decrease with increased metal complex loading on electrode surfaces.[67–69] Fig. 8b shows CVs of the different loadings of FePOMe immobilised on the me-ATO electrodes under Ar and in O_2 under turnover conditions. Remarkably, under Ar, reversible peaks for the Fe^{2+}/Fe^{3+} redox couple can be observed (which is usually not the case in aqueous media), albeit with very broad FWHMs. For the higher loading of FePOMe, the FWHMs are broader and there is a positive shift in the redox potential $E_{1/2}$ of almost 70 mV, which corresponds to a shift in the ORR onset potential of 75 mV. It has been shown for numerous redox species (including porphyrins) immobilised on metal and semiconducting surfaces that $E_{1/2}$ increases with surface coverage[70–73], as predicted by models such as the surface activity model of Brown and Anson.[74] In this model, the free energy for the redox transition depends on lateral interactions between oxidised and reduced species. In the case of the immobilised FePOMe, intermolecular repulsion between +3 oxidised species is greater than between the catalytically active reduced +2 species. Thus, as the loading of FePOMe increases, the thermodynamic driving force for the reduction of +3 species, and thereby the ORR, increases. Such a shift in $E_{1/2}$ is not observed in acetonitrile, which can be explained by an increase in ion pairing strength between the FePOMe and the perchlorate anion, or the intercalation of the less polar acetonitrile solvent molecules between the immobilised species, both of which would minimise intermolecular repulsion.[75] This is also reflected in the narrower FWHMs measured in acetonitrile compared to water.

The highest activity for FePOMe immobilised on me-ATO was obtained in 0.1 M KOH (pH 12.8) with an onset potential of 810 mV (vs RHE) (Fig. S20). This compares well to the best previously reported onset potentials of 922 and 913 mV (vs RHE) for axial-pyridine coordinated iron phthalocyanine[19], or axial-imidazole coordinated iron porphyrin immobilised on CNTs, respectively.[20] Other studies on carbon electrodes have reported onset potentials of 820 mV and 880 mV.[76,77] Considering the low loading of catalyst present in the herein presented me-ATO system (3.5 µg/cm^2 of FePOMe), which is about two orders of magnitude less than the loadings employed in the aforementioned systems (between 200 µg/cm^2 and 1 mg/cm^2), the obtained onset potential compare well with results from literature.

'Post-coordination' on me-ATO resulted in the most stable overpotentials and, thus, chronoamperometric measurements were recorded at a potential of 0.32 V (vs RHE), with measurements conducted before and after incubation with FePOMe. As seen in Fig. 9, there is a decrease in activity over

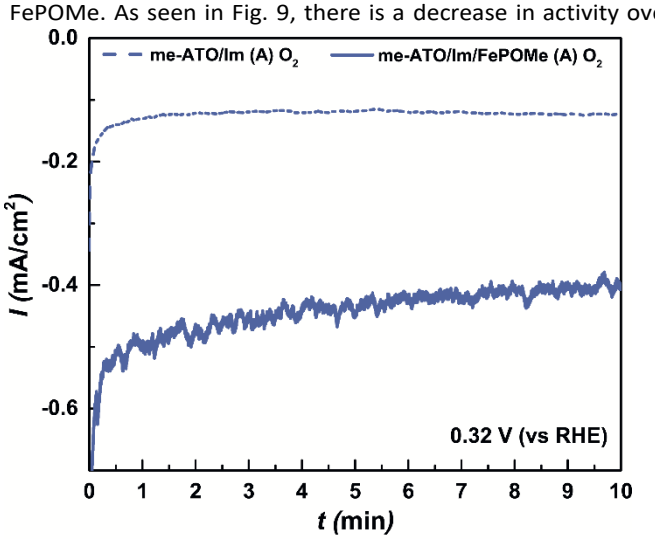

Figure 9 Chronoamperometric measurements at 0.32 V (vs RHE) under O_2 bubbling of FePOMe immobilised on me-ATO using 'post-coordination'.

time (a further, extended measurement is shown in Fig. S21), which could result from three things: (a) desorption of the interface linker molecules, (b) a disruption of the linker-catalyst axial coordination (e.g. due to protonation of the imine nitrogen on the linker imidazole ring, or a change in orbital overlap resulting from the formation of intermediate Fe oxo-species during catalysis), or (c) deactivation of the immobilised FePOMe catalyst (e.g. due to the formation of superoxides during catalysis). While the reason for deactivation remains so far unclear, CVs of me-ATO electrodes modified using the 'post-coordination' method show that the resulting decrease in Γ_{CV} for the FePOMe Fe^{2+}/Fe^{3+} couple could be restored by re-incubating the electrode in 1 mM FePOMe in acetonitrile (Fig. S22), effectively reloading the imidazole-terminated interface with FePOMe. This result therefore emphasises the robustness of the interface itself and rules out its desorption from the oxide surface; a result which is corroborated by the ATR-IR spectroelectrochemical stability measurements.

Discussion

The apparent fast electron transfer rates of the immobilised redox species and high stabilities observed for the herein presented electrografted diazonium interfaces likely result from its binding motif, which differs from other anchoring groups, such as non-covalent phosphonates, carboxylates and hydroxamates etc., or covalently bound silanes and their derivatives. Experimental and theoretical studies on TiO_2 have shown that organic carboxylate and hydroxamate anchoring groups exhibit faster interfacial electron transfer because of a better electronic coupling at the oxide interface compared to phosphonate anchoring groups.[16–18] This latter poor coupling may arise from the tetrahedral geometry of the phosphorous atom and the loss of conjugation through to the oxide.[78] At the expense of their electronic behaviour, phosphonate and silane-derived anchoring groups exhibit greater stabilities, with phosphonate anchoring groups showing stabilities that are orders of magnitude greater than carboxylate anchoring groups.[79,80] That being said, phosphonates still show poor stabilities in pH's above 5 or 6, thus limiting their application in certain reactions, while silane-derived species result in covalent bonds which are stronger and have been shown to be stable up to pH 11.[12,14,80,81] It is tentatively proposed that the strong M-O-C bond formed upon electrografting of diazonium salts on oxide surfaces not only results in good electronic coupling with immobilised molecular redox species, but also provides high chemical and electrochemical stabilities.

Conclusions

The electrografting of diazonium salts onto TCO materials was explored as a stable alternative to conventional anchoring groups for immobilising molecular species such electrocatalysts and photosensitisers. To this end, surface sensitive *in situ* ATR-IR spectroscopy in combination with spectroelectrochemistry was used as a tool to provide unprecedented information on the interface formation, structure and stability not achievable using conventional UV-Vis or electrochemical techniques. Interfaces electrografted on a model oxide - mesoporous ATO – were shown to be stable in a wide hydrolytic (pH range ca. 2.5 – 12) and electrochemical stability window (ranging from at least -0.73 to 2.23 V vs RHE in aqueous media) making them excellent candidates for a wide range of electrocatalytic energy conversion and storage applications, especially the OER, which typically operates under alkaline conditions when catalysed using non-precious metal-based compounds e.g. cobalt- or nickel-based catalysts[82]. Furthermore, the stability of the interface in organic media (ranging from -1.3 V to at least 1.6 V vs Fc/Fc^+ in acetonitrile) also makes them suitible electrocatalytic organic synthesis. *In situ* IR spectroscopy is thus shown to be a powerful tool for researchers working on oxide-based electrochemical devices, such as electrolyzers, photoelectrochemical or dye-sensitised solar cells, or sensors, i.e. anywhere molecular-inorganic interfaces play an important role in a device's performance. As a model electrocatalyst, an Fe hangman porphyrin that is active for the ORR was immobilised on both pl-ITO and me-ATO using electrografting, with surface coverages comparable to those reported using other anchoring groups. Fast electron transfer rates between the electrodes and the immobilised species were demonstrated, with *in situ* rR spectroelectrochemistry used on me-ATO to determine their coordination and demonstrate their excellent electrochemical accessibility. The best onset potential for the ORR achieved using this system was 810 mV (vs RHE), which, despite the ultra-low loading applied, is close to reported potentials obtained for similar catalysts immobilised on carbon electrodes.

Conflicts of interest

There are no conflicts to declare.

Acknowledgements

This work was funded by the DFG, the cluster of excellence UniCat (EXC 314), its Berlin International Graduate School of Natural Sciences and Engineering BIG-NSE, as well as the University of Freiburg and the BMBF (FKZ 01FP13033F).

References

(1) Connolly, D.; Mathiesen, B. V; Ridjan, I. A Comparison between Renewable Transport Fuels That Can Supplement or Replace Biofuels in a 100% Renewable Energy System. *Energy* **2014**, *73*, 110–125.

(2) Vojvodic, A.; Nørskov, J. K. Special Topic : Catalysis — Facing the Future New Design Paradigm for Heterogeneous Catalysts. *Natl. Sci. Rev.* **2015**, *2* (2), 140–143.

(3) She, Z. W.; Kibsgaard, J.; Dickens, C. F.; Chorkendorff, I.; Nørskov, J. K.; Jaramillo, T. F. Combining Theory and Experiment in Electrocatalysis: Insights into Materials Design. *Science*. 2017.

(4) Reuillard, B.; Ly, K. H.; Rosser, T. E.; Kuehnel, M. F.; Zebger, I.; Reisner, E. Tuning Product Selectivity for Aqueous CO2 Reduction with a Mn(bipyridine)-Pyrene Catalyst Immobilized on a Carbon Nanotube Electrode. *J. Am. Chem. Soc.* **2017**, *139* (41), 14425–14435.

(5) Bullock, R. M.; Das, A. K.; Appel, A. M. Surface Immobilization of Molecular Electrocatalysts for Energy Conversion. *Chem. - A Eur. J.* **2017**, *23* (32), 7626–7641.

(6) Wang, M.; Yang, Y.; Shen, J.; Jiang, J.; Sun, L. Visible-Light-Absorbing Semiconductor/molecular Catalyst Hybrid Photoelectrodes for H 2 or O 2 Evolution: Recent Advances and Challenges. *Sustain. Energy Fuels* **2017**, *1* (8), 1641–1663.

(7) Rosser, T. E.; Gross, M. A.; Lai, Y.-H.; Reisner, E. Precious-Metal Free Photoelectrochemical Water Splitting with Immobilised Molecular Ni and Fe Redox Catalysts. *Chem. Sci.* **2016**, *7*, 4024–4035.

(8) Odrobina, J.; Scholz, J.; Pannwitz, A.; Francàs, L.; Dechert, S.; Llobet, A.; Jooss, C.; Meyer, F. Backbone Immobilization of the Bis(bipyridyl)pyrazolate Diruthenium Catalyst for Electrochemical Water Oxidation. *ACS Catal.* **2017**, *7* (3), 2116–2125.

(9) Brennaman, M. K.; Dillon, R. J.; Alibabaei, L.; Gish, M. K.; Dares, C. J.; Ashford, D. L.; House, R. L.; Meyer, G. J.; Papanikolas, J. M.; Meyer, T. J. Finding the Way to Solar Fuels with Dye-Sensitized Photoelectrosynthesis Cells. *J. Am. Chem. Soc.* **2016**, *138* (40), 13085–13102.

(10) Willkomm, J.; Orchard, K. L.; Reynal, A.; Pastor, E.; Durrant, J. R.; Reisner, E. Dye-Sensitised Semiconductors Modified with Molecular Catalysts for Light-Driven H 2 Production. *Chem. Soc. Rev* **2016**, *45* (1), 9–23.

(11) Materna, K. L.; Rudshteyn, B.; Brennan, B. J.; Kane, M. H.; Bloomfield, A. J.; Huang, D. L.; Shopov, D. Y.; Batista, V. S.; Crabtree, R. H.; Brudvig, G. W. Heterogenized Iridium Water-Oxidation Catalyst from a Silatrane Precursor. *ACS Catal.* **2016**, *6* (8), 5371–5377.

(12) Materna, K. L.; Brennan, B. J.; Brudvig, G. W. Silatranes for Binding Inorganic Complexes to Metal Oxide Surfaces. *Dalt. Trans.* **2015**, *44* (47), 20312–20315.

(13) McNamara, W. R.; Snoeberger, R. C.; Li, G.; Schleicher, J. M.; Cady, C. W.; Poyatos, M.; Schmuttenmaer, C. A.; Crabtree, R. H.; Brudvig, G. W.; Batista, V. S. Acetylacetonate Anchors for Robust Functionalization of TiO2 Nanoparticles with Mn(II)-Terpyridine Complexes. *J. Am. Chem. Soc.* **2008**, *130* (43), 14329–14338.

(14) Brennan, B. J.; Llansola Portolés, M. J.; Liddell, P. A.; Moore, T. A.; Moore, A. L.; Gust, D. Comparison of Silatrane, Phosphonic Acid, and Carboxylic Acid Functional Groups for Attachment of Porphyrin Sensitizers to TiO2 in Photoelectrochemical Cells. *Phys. Chem. Chem. Phys.* **2013**, *15* (39), 16605.

(15) Li, F.; Fan, K.; Xu, B.; Gabrielsson, E.; Daniel, Q.; Li, L.; Sun, L. Organic Dye-Sensitized Tandem Photoelectrochemical Cell for Light Driven Total Water Splitting. *J. Am. Chem. Soc.* **2015**, *137* (28), 9153–9159.

(16) Negre, C. F. A.; Milot, R. L.; Martini, L. A.; Ding, W.; Crabtree, R. H.; Schmuttenmaer, C. A.; Batista, V. S. Efficiency of Interfacial Electron Transfer from Zn-Porphyrin Dyes into TiO2correlated to the Linker Single Molecule Conductance. *J. Phys. Chem. C* **2013**, *117* (46), 24462–24470.

(17) Li, W.; Rego, L. G. C.; Bai, F. Q.; Wang, J.; Jia, R.; Xie, L. M.; Zhang, H. X. What Makes Hydroxamate a Promising Anchoring Group in Dye-Sensitized Solar Cells? Insights from Theoretical Investigation. *J. Phys. Chem. Lett.* **2014**, *5* (22), 3992–3999.

(18) Martini, L. A.; Moore, G. F.; Milot, R. L.; Cai, L. Z.; Sheehan, S. W.; Schmuttenmaer, C. A.; Brudvig, G. W.; Crabtree, R. H. Modular Assembly of High-Potential Zinc Porphyrin Photosensitizers Attached to TiO2 with a Series of Anchoring Groups. *J. Phys. Chem. C* **2013**, *117* (28), 14526–14533.

(19) Cao, R.; Thapa, R.; Kim, H.; Xu, X.; Gyu Kim, M.; Li, Q.; Park, N.; Liu, M.; Cho, J. Promotion of Oxygen Reduction by a Bio-Inspired Tethered Iron Phthalocyanine Carbon Nanotube-Based Catalyst. *Nat. Commun.* **2013**, *4* (May), 2076.

(20) Wei, P. J.; Yu, G. Q.; Naruta, Y.; Liu, J. G. Covalent Grafting of Carbon Nanotubes with a Biomimetic Heme Model Compound to Enhance Oxygen Reduction Reactions. *Angew. Chemie - Int. Ed.* **2014**, *53* (26), 6659–6663.

(21) Elgrishi, N.; Griveau, S.; Chambers, M. B.; Bedioui, F.; Fontecave, M. Versatile Functionalization of Carbon Electrodes with a Polypyridine Ligand: Metallation and Electrocatalytic H(+) and CO2 Reduction. *Chem. Commun.* **2015**, *51* (14), 2995–2998.

(22) Maurin, A.; Robert, M. Catalytic CO 2 -to-CO Conversion in Water by Covalently Functionalized Carbon Nanotubes with a Molecular Iron Catalyst. *Chem. Commun.* **2016**, *52* (81), 12084–12087.

(23) Mahouche-Chergui, S.; Gam-Derouich, S.; Mangeney, C.;

Chehimi, M. M. Aryl Diazonium Salts: A New Class of Coupling Agents for Bonding Polymers, Biomacromolecules and Nanoparticles to Surfaces. *Chem. Soc. Rev.* **2011**, *40* (7), 4143–4166.

(24) Goff, A. Le; Artero, V.; Jousselme, B.; Tran, P. D.; Guillet, N.; Métayé, R.; Fihri, A.; Palacin, S.; Fontecave, M. From Hydrogenases to Noble Metal-Free Catalytic Nanomaterials for H2production and Uptake. *Science* **2009**, *326* (5958), 1384–1387.

(25) Chehimi, M. M. Aryl Diazonium Salts : New Coupling Agents in Polymer and Surface Science. Wiley-VCH: Weinheim 2012.

(26) Cottineau, T.; Morin, M.; Bélanger, D. Surface Band Structure of Aryl-Diazonium Modified P-Si Electrodes Determined by X-Ray Photoelectron Spectroscopy and Electrochemical Measurements. *RSC Adv.* **2013**, *3* (45), 23649.

(27) Palacin, S.; Bureau, C.; Charlier, J.; Deniau, G.; Mouanda, B.; Viel, P. Molecule-to-Metal Bonds: Electrografting Polymers on Conducting Surfaces. *ChemPhysChem*. WILEY-VCH Verlag October 18, 2004, pp 1468–1481.

(28) Charlton, M. R.; Suhr, K. J.; Holliday, B. J.; Stevenson, K. J. Electrochemical Modification of Indium Tin Oxide Using Di(4-Nitrophenyl) Iodonium Tetrafluoroborate. *Langmuir* **2015**, *31* (2), 695–702.

(29) Lund, T.; Nguyen, P. T.; Ruhland, T. Electrochemical Grafting of TiO2-Based Photo-Anodes and Its Effect in Dye-Sensitized Solar Cells. *J. Electroanal. Chem.* **2015**, *758*, 85–92.

(30) Merson, A.; Dittrich, T.; Zidon, Y.; Rappich, J.; Shapira, Y. Charge Transfer from TiO2 into Adsorbed Benzene Diazonium Compounds. *Appl. Phys. Lett.* **2004**, *85* (6), 1075–1076.

(31) Cao, L.; Fang, G.; Wang, Y. Electroreduction of Viologen Phenyl Diazonium Salts as a Strategy to Control Viologen Coverage on Electrodes. *Langmuir* **2017**, *33* (4), 980–987.

(32) Maldonado, S.; Smith, T. J.; Williams, R. D.; Morin, S.; Barton, E.; Stevenson, K. J. Surface Modification of Indium Tin Oxide via Electrochemical Reduction of Aryldiazonium Cations. *Langmuir* **2006**, *22* (6), 2884–2891.

(33) Rawson, F. J.; Yeung, C. L.; Jackson, S. K.; Mendes, P. M. Tailoring 3D Single-Walled Carbon Nanotubes Anchored to Indium Tin Oxide for Natural Cellular Uptake and Intracellular Sensing. *Nano Lett.* **2013**, *13* (1), 1–8.

(34) Hebié, S.; Devillers, C. H.; Fournier, S.; Lucas, D. Direct Grafting of Free-Base Meso-Triarylporphyrins on Electrode Materials through Diazonium Reduction: Reversible Zinc(II) Metallation of the Resulting Materials. *ChemElectroChem* **2016**, *3* (1), 45–50.

(35) Lamberti, F.; Agnoli, S.; Brigo, L.; Granozzi, G.; Giomo, M.; Elvassore, N. Surface Functionalization of Fluorine-Doped Tin Oxide Samples through Electrochemical Grafting. *ACS Appl. Mater. Interfaces* **2013**, *5* (24), 12887–12894.

(36) Harris, T. G. A. A.; Heidary, N.; Kozuch, J.; Frielingsdorf, S.; Lenz, O.; Mroginski, M.-A.; Hildebrandt, P.; Zebger, I.; Fischer, A. In Situ Spectroelectrochemical Studies into the Formation and Stability of Robust Diazonium-Derived Interfaces on Gold Electrodes for the Immobilization of an Oxygen-Tolerant Hydrogenase. *ACS Appl. Mater. Interfaces* **2018**. 10.1021/acsami.8b02273

(37) Hanson, K.; Brennaman, M. K.; Luo, H.; Glasson, C. R. K.; Concepcion, J. J.; Song, W.; Meyer, T. J. Photostability of Phosphonate-Derivatized, Ru II Polypyridyl Complexes on Metal Oxide Surfaces. *ACS Appl. Mater. Interfaces* **2012**, *4* (3), 1462–1469.

(38) Hyde, J. T.; Hanson, K.; Vannucci, A. K.; Lapides, A. M.; Alibabaei, L.; Norris, M. R.; Meyer, T. J.; Harrison, D. P. Electrochemical Instability of Phosphonate-Derivatized, ruthenium(III) Polypyridyl Complexes on Metal Oxide Surfaces. *ACS Appl. Mater. Interfaces* **2015**, *7* (18), 9554–9562.

(39) Frasca, S.; Molero Milan, A.; Guiet, A.; Goebel, C.; Pérez-Caballero, F.; Stiba, K.; Leimkühler, S.; Fischer, A.; Wollenberger, U. Bioelectrocatalysis at Mesoporous Antimony Doped Tin Oxide electrodes—Electrochemical Characterization and Direct Enzyme Communication. *Electrochim. Acta* **2013**, *110*, 172–180.

(40) Luo, H.; Fang, Z.; Song, N.; Garvey, T.; Lopez, R.; Meyer, T. J. High Surface Area Antimony-Doped Tin Oxide Electrodes Templated by Graft Copolymerization. Applications in Electrochemical and Photoelectrochemical Catalysis. *ACS Appl. Mater. Interfaces* **2015**, *7* (45), 25121–25128.

(41) Oh, H. S.; Nong, H. N.; Strasser, P. Preparation of Mesoporous Sb-, F-, and in-Doped SnO2bulk Powder with High Surface Area for Use as Catalyst Supports in Electrolytic Cells. *Adv. Funct. Mater.* **2015**, *25* (7), 1074–1081.

(42) Oh, H.-S.; Nong, H. N.; Reier, T.; Gliech, M.; Strasser, P. Oxide-Supported Ir Nanodendrites with High Activity and Durability for the Oxygen Evolution Reaction in Acid PEM Water Electrolyzers. *Chem. Sci.* **2015**, *6* (6), 3321–3328.

(43) Peters, K.; Lokupitiya, H. N.; Sarauli, D.; Labs, M.; Pribil, M.; Rathousky, J.; Kuhn, A.; Leister, D.; Stefik, M.; Fattakhova-Rohlfing, D. Nanostructured Antimony-Doped Tin Oxide Layers with Tunable Pore Architectures as Versatile Transparent Current Collectors for Biophotovoltaics. *Adv. Funct. Mater.* **2016**, *26* (37), 6682–6692.

(44) Neumann, B.; Kielb, P.; Rustam, L.; Fischer, A.; Weidinger, I. M.; Wollenberger, U. Bioelectrocatalytic Reduction of Hydrogen Peroxide by Microperoxidase-11 Immobilized on Mesoporous Antimony-Doped Tin Oxide. *ChemElectroChem* **2017**, *4* (4), 913–919.

(45) Alibabaei, L.; Brennaman, M. K.; Norris, M. R.; Kalanyan, B.; Song, W.; Losego, M. D.; Concepcion, J. J.; Binstead, R. A.; Parsons, G. N.; Meyer, T. J. Solar Water Splitting in a Molecular Photoelectrochemical Cell. *Proc. Natl. Acad. Sci.* **2013**, *110* (50), 20008–20013.

(46) Willkomm, J.; Muresan, N. M.; Reisner, E. Enhancing H 2 Evolution Performance of an Immobilised Cobalt Catalyst by Rational Ligand Design. *Chem. Sci.* **2015**, *6* (5), 2727–2736.

(47) Menanteau, T.; Levillain, E.; Downard, A. J.; Breton, T. Evidence of Monolayer Formation via Diazonium Grafting with a Radical Scavenger: Electrochemical, AFM and XPS

Monitoring. *Phys. Chem. Chem. Phys.* **2015**, *17* (19), 13137–13142.

(48) Tian, R.; Zhang, Y.; Chen, Z.; Duan, H.; Xu, B.; Guo, Y.; Kang, H.; Li, H.; Liu, H. The Effect of Annealing on a 3D SnO2/graphene Foam as an Advanced Lithium-Ion Battery Anode. *Sci. Rep.* **2016**, *6*, 1–9.

(49) Brinker, C. J. Hydrolysis and Condensation of Silicates: Effects on Structure. *Journal of Non-Crystalline Solids*. 1988, pp 31–50.

(50) Garrett, D. J.; Jenkins, P.; Polson, M. I. J.; Leech, D.; Baronian, K. H. R.; Downard, A. J. Diazonium Salt Derivatives of Osmium Bipyridine Complexes: Electrochemical Grafting and Characterisation of Modified Surfaces. *Electrochim. Acta* **2011**, *56* (5), 2213–2220.

(51) Benck, J. D.; Pinaud, B. A.; Gorlin, Y.; Jaramillo, T. F. Substrate Selection for Fundamental Studies of Electrocatalysts and Photoelectrodes: Inert Potential Windows in Acidic, Neutral, and Basic Electrolyte. *PLoS One* **2014**, *9* (10), e107942.

(52) Yeh, C. Y.; Chang, C. J.; Nocera, D. G. "Hangman" porphyrins for the Assembly of a Model Heme Water Channel. *J. Am. Chem. Soc.* **2001**, *123* (7), 1513–1514.

(53) Chang, C. J.; Chng, L. L.; Nocera, D. G. Proton-Coupled O-O Activation on a Redox Platform Bearing a Hydrogen-Bonding Scaffold. *J. Am. Chem. Soc.* **2003**, *125* (7), 1866–1876.

(54) Soper, J. D.; Kryatov, S. V.; Rybak-Akimova, E. V.; Nocera, D. G. Proton-Directed Redox Control of O-O Bond Activation by Heme Hydroperoxidase Models. *J. Am. Chem. Soc.* **2007**, *129* (16), 5069–5075.

(55) Graham, D. J.; Dogutan, D. K.; Schwalbe, M.; Nocera, D. G. Hangman Effect on Hydrogen Peroxide Dismutation by Fe(iii) Corroles. *Chem. Commun.* **2012**, *48* (35), 4175.

(56) Ly, H. K.; Wrzolek, P.; Heidary, N.; Götz, R.; Horch, M.; Kozuch, J.; Schwalbe, M.; Weidinger, I. M. 2 Nd Coordination Sphere Controlled Electron Transfer of Iron Hangman Complexes on Electrodes Probed by Surface Enhanced Vibrational Spectroscopy. *Chem. Sci.* **2015**, *6* (12), 6999–7007.

(57) Wrzolek, P.; Wahl, S.; Schwalbe, M. Electrocatalytic Investigation on the Water Oxidation Ability of a Hangman Complex Based on the [Ru(tpy)(bpy)(OH2)]2+ Motif. *Catal. Today* **2017**, *290*, 28–32.

(58) Bard, A. J.; Faulkner, L. R. *Electrochemical Methods: Fundamentals and Applications, 2nd Edition*; John Wiley & Sons: New York, 2001.

(59) Laviron, E. The Use of Linear Potential Sweep Voltammetry and of A.c. Voltammetry for the Study of the Surface Electrochemical Reaction of Strongly Adsorbed Systems and of Redox Modified Electrodes. *J. Electroanal. Chem.* **1979**, *100* (1–2), 263–270.

(60) Galloni, P.; Vecchi, A.; Coletti, A.; Gatto, E.; Floris, B.; Conte, V. Porphyrins as Active Components for Electrochemical and Photoelectrochemical Devices. In *Handbook of Porphyrin Science*; Handbook of Porphyrin Science; World Scientific Publishing Company: Singapore, 2012; Vol. 33, pp 225–415.

(61) Roth, K. M.; Yasseri, A. A.; Liu, Z.; Dabke, R. B.; Malinovskii, V.; Schweikart, K. H.; Yu, L.; Tiznado, H.; Zaera, F.; Lindsey, J. S.; Kuhr, W. G.; Bocian, D. F. Measurements of Electron-Transfer Rates of Charge-Storage Molecular Monolayers on Si(100). Toward Hybrid Molecular/semiconductor Information Storage Devices. *J. Am. Chem. Soc.* **2003**, *125* (2), 505–517.

(62) Laviron, E. General Expression of the Linear Potential Sweep Voltammogram in the Case of Diffusionless Electrochemical Systems. *J. Electroanal. Chem. Interfacial Electrochem.* **1979**, *101*, 19–28.

(63) Ye, J. S.; Wen, Y.; Zhang, W. De; Cui, H. F.; Gan, L. M.; Xu, G. Q.; Sheu, F. S. Application of Multi-Walled Carbon Nanotubes Functionalized with Hemin for Oxygen Detection in Neutral Solution. *J. Electroanal. Chem.* **2004**, *562* (2), 241–246.

(64) Feng, Z.; Sagara, T.; Niki, K. Application of Potential-Modulated UV-Visible Reflectance Spectroscopy to Electron Transfer Rate Measurements for Adsorbed Species on Electrode Surfaces. *Anal. Chem.* **1995**, *67* (14), 3564–3570.

(65) Chen, Z.; Concepcion, J. J.; Jurss, J. W.; Meyer, T. J. Single-Site, Catalytic Water Oxidation on Oxide Surfaces. *J. Am. Chem. Soc.* **2009**, *131* (43), 15580–15581.

(66) Hoertz, P. G.; Chen, Z.; Kent, C. A.; Meyer, T. J. Application of High Surface Area Tin-Doped Indium Oxide Nanoparticle Films as Transparent Conducting Electrodes. *Inorg. Chem.* **2010**, *49* (18), 8179–8181.

(67) Elzing, A.; van der Putten, A.; Visscher, W.; Barendrecht, E. The Cathodic Reduction of Oxygen at Cobalt Phthalocyanine. *J. Electroanal. Chem. Interfacial Electrochem.* **1986**, *200* (1–2), 313–322.

(68) Elzing, A.; van der Putten, A.; Visscher, W.; Barendrecht, E. The Cathodic Reduction of Oxygen at Cobalt Phthalocyanine. Influence of Electrode Preparation on Electrocatalysis. *J. Electroanal. Chem.* **1986**, *200* (1–2), 313–322.

(69) Zagal, J. H.; Bedioui, F.; Dodelet, J.-P. *N4-Macrocyclic Metal Complexes*; Springer Science & Business Media: New York, 2006.

(70) Acevedo, D.; Abruña, H. D. Electron-Transfer Study and Solvent Effects on the Formal Potential of a Redox-Active Self-Assembling Monolayer. *J. Phys. Chem.* **1991**, *95* (23), 9590–9594.

(71) Roth, K. M.; Gryko, D. T.; Clausen, C.; Li, J.; Lindsey, J. S.; Kuhr, W. G.; Bocian, D. F. Comparison of Electron-Transfer and Charge-Retention Characteristics of Porphyrin-Containing Self-Assembled Monolayers Designed for Molecular Information Storage. *J. Phys. Chem. B* **2002**, *106* (34), 8639–8648.

(72) Yasseri, A. A.; Syomin, D.; Loewe, R. S.; Laha, J. K.; Lindsey, J. S.; Zaera, F.; Bocian, D. F. Structural and Electron-Transfer Characteristics of O-, S-, and Se-Tethered Porphyrin Monolayers on Si(100). *Journal of the American Chemical Society*. 2005, pp 15603–15612.

(73) Jiao, J.; Nordlund, E.; Lindsey, J. S.; Bocian, D. F. Effects of Counterion Mobility, Surface Morphology, and Charge

Screening on the Electron-Transfer Rates of Porphyrin Monolayers. *J. Phys. Chem. C* **2008**, *112* (15), 6173–6180.

(74) Brown, A. P.; Anson, F. C. Cyclic and Differential Pulse Voltammetric Behavior of Reactants Confined to the Electrode Surface. *Anal. Chem.* **1977**, *49* (11), 1589–1595.

(75) Eberspacher, T. A.; Collman, J. P.; Chidsey, C. E. D.; Donohue, D. L.; Ryswyk, H. Van. Modular Assembly and Air-Stable Electrochemistry of Ruthenium Porphyrin Monolayers. *Langmuir* **2003**, *19* (9), 3814–3821.

(76) Thorum, M. S.; Hankett, J. M.; Gewirth, A. A. Poisoning the Oxygen Reduction Reaction on Carbon-Supported Fe and Cu Electrocatalysts: Evidence for Metal-Centered Activity. *J. Phys. Chem. Lett.* **2011**, *2* (4), 295–298.

(77) Chen, R.; Li, H.; Chu, D.; Wang, G. Unraveling Oxygen Reduction Reaction Mechanisms on Carbon-Supported Fe-Phthalocyanine and Co-Phthalocyanine Catalysts in Alkaline Solutions. *J. Phys. Chem. C* **2009**, *113* (48), 20689–20697.

(78) Guerrero, G.; Alauzun, J. G.; Granier, M.; Laurencin, D.; Mutin, P. H. Phosphonate Coupling Molecules for the Control of Surface/interface Properties and the Synthesis of Nanomaterials. *Dalt. Trans.* **2013**, *42* (35), 12569–12585.

(79) Péchy, P.; Rotzinger, F. P.; Nazeeruddin, M. K.; Kohle, O.; Zakeeruddin, S. M.; Humphry-Baker, R.; Grätzel, M. Preparation of Phosphonated Polypyridyl Ligands to Anchor Transition-Metal Complexes on Oxide Surfaces: Application for the Conversion of Light to Electricity with Nanocrystalline TiO 2 Films. *J. Chem. Soc., Chem. Commun.* **1995**, *0* (1), 65–66.

(80) Gillaizeau-Gauthier, I.; Odobel, F.; Alebbi, M.; Argazzi, R.; Costa, E.; Bignozzi, C. A.; Qu, P.; Meyer, G. J. Phosphonate-Based Bipyridine Dyes for Stable Photovoltaic Devices. *Inorg. Chem.* **2001**, *40* (23), 6073–6079.

(81) Bae, E.; Choi, W.; Park, J.; Shin, H. S.; Kim, S. Bin; Lee, J. S. Effects of Surface Anchoring Groups (Carboxylate vs Phosphonate) in Ruthenium-Complex-Sensitized TiO2 on Visible Light Reactivity in Aqueous Suspensions. *J. Phys. Chem. B* **2004**, *108* (37), 14093–14101.

(82) Blakemore, J. D.; Crabtree, R. H.; Brudvig, G. W. Molecular Catalysts for Water Oxidation. *Chem. Rev.* **2015**.